Sensitivity analysis and characterization of the uncertain input data for the EXPERT vehicle

Julie Tryoen, Pietro Marco Congedo, Remi Abgrall, Thierry E. Magin, Nadège Villedieu

Sensitivity analysis and characterization of the uncertain input data for the EXPERT vehicle

Julie Tryoen, Pietro Marco Congedo, Rémi Abgrall, Thierry Magin, Nadege Villedieu

RESEARCH REPORT

N° 8360

Septembre 2013

Project-Teams BACCHUS

ISSN 0249-6399 ISRN INRIA/RR--8360--FR+ENG

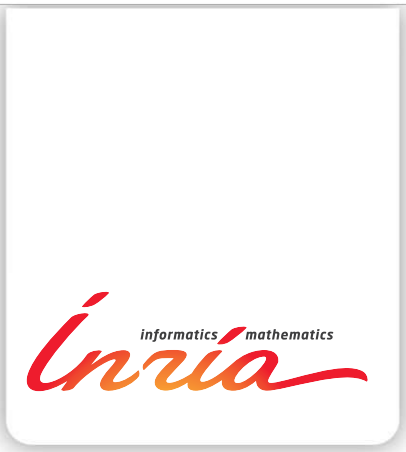

Sensitivity analysis and characterization of the uncertain input data for the EXPERT vehicle

Julie Tryoen*, Pietro Marco Congedo*, Rémi Abgrall*, Thierry Magin†, Nadege Villedieu†

Project-Teams BACCHUS

Research Report n° 8360 — Septembre 2013 — 18 pages

Abstract: The paper investigates a new methodology to rebuild freestream conditions for the trajectory of a re-entry vehicle from measurements of stagnation-point pressure and heat flux. Uncertainties due to measurements and model parameters are taken into account and a Bayesian setting is used to solve the associated stochastic inverse problem. A sensitivity analysis based on a stochastic spectral framework is first investigated to study the impact of uncertain input data on stagnation-point measurements. An original backward uncertainty propagation method is then proposed, for which only the uncertainties that have the most impact are retained.

Key-words: experimental uncertainty, inverse problem, bayesian methods, re-entry vehicle, polynomial chaos methods

* INRIA Bordeaux Sud-Ouest
† von Karmann Institute for Fluid Dynamics, 1640 Rhode-Saint-Genèse, Belgium

RESEARCH CENTRE
BORDEAUX – SUD-OUEST

351, Cours de la Libération
Bâtiment A 29
33405 Talence Cedex

Sensitivity analysis and characterization of the uncertain input data for the EXPERT vehicle

Résumé : Ce papier est focalisé sur une nouvelle méthode pour reconstruire les conditions de freestream d'un véhicule de rentrée en partant des mesures sur la pression et le flux de chaleur au point de stagnation. Les incertitudes dues aux mesures et aux paramètres du modèle sont prises en compte et une approche de type bayésienne est utilisée pour résoudre le problème inverse stochastique. Une étude de sensibilité est utilisée pour évaluer l'impact des données d'input incertaines sur les mesures au point de stagnation. Une méthode de propagation 'backward' est proposée, en considérant seulement les incertitudes qui ont l'impact le plus important.

Mots-clés : incertitudes sur les données expérimentales, problème inverse, approche bayésienne, rentrée atmosphérique, méthodes spectrales, polynomes de Chaos

1 Introduction

Simulation of atmospheric entries of spacecraft is a challenging problem involving many complex physical phenomena, including rarefied gas effects, aerothermochemistry, radiation, and the response of thermal protection materials to extreme conditions. The availability of powerful computational resources and general-purpose numerical algorithms creates increasing opportunities to perform multiphysics simulations of complex systems, in particular in aerospace science. Reliable predictions require sophisticated physico-chemical models as well as a systematic and comprehensive treatment of model calibration and validation, including the quantification of inherent model uncertainties.

Conventionally, engineers resort to safety factors to avoid space-mission failure. At the interface of physics, mathematics, and computer science, Uncertainty Quantification (UQ) aims at developing a more rigorous framework and more reliable methods to characterize the impact of uncertainties on the prediction of Quantities Of Interest (QOI). Some uncertainties arise from the physical simplifications made to obtain a mathematical model representative of the complex phenomena studied [1]; others come from the numerical approximations due to the finite discretization used in the numerical solver for approximating the solution of the mathematical model. In the sequel, we will not account for modeling and numerical uncertainties. Our interest lies in uncertainties associated to a limited knowledge or an intrinsic variability of the input quantities required for performing the analysis. For instance, numerical simulations need the precise specification of boundary conditions and model parameters, such as reaction rate coefficients, and typically only limited information is available from corresponding experiments and observations.

The post-flight analysis of a space mission requires accurate determination of the freestream conditions for the trajectory, that is, temperature and pressure conditions and the Mach number in front of the shock. These quantities can be rebuilt from the pressure and heat flux measured on the spacecraft by means of a Flush Air Data System (FADS) [2]. This instrumentation comprises a set of sensors flush mounted in the thermal protection system to measure the static pressure (pressure taps) and heat flux (calorimeters) (see Figure 1). As shown by zur Nieden and Olivier [3], state of the art techniques for freestream characterization rely on several approximations, such as the equivalent specific heat ratio approximation, which means that one replaces a complex high temperature effect possibly including thermo-chemical non-equilibrium by an "equivalent" calorically perfect gas. This approximation is then used, starting from sensors measurements, to reconstruct freestream conditions and prescribe error intervals on these quantities. These techniques do not yet integrate measurement errors nor the heat flux contribution, for which a correct knowledge drives more complex models such as gas surface interaction. In this context, Computational Fluid Dynamics (CFD) supplied with UQ tools permits to take into account chemical effects and to include both measurement errors and epistemic uncertainties on the chemical model parameters in the bulk and at the wall (surface catalysis). Rebuilding the freestream conditions from the FADS data therefore amounts to solving a stochastic inverse problem.

The forward problem, which consists in predicting stagnation-point pressure and heat flux from freestream conditions, is described by a physico-chemical model and solved by suitable numerical methods proposed by Barbante [4, 5]. We investigate one point of the trajectory of the European EXPerimental Reentry Test-bed (EXPERT) vehicle, which has been developed by the European Space Agency as part of its General Technological Research Program [6]. The trajectory point corresponds roughly to the chemical non-equilibrium flow conditions of Table 1. The inverse problem is then reduced to determine for instance only freestream pressure and Mach number. The purpose of this paper is to propose a new methodology for solving the

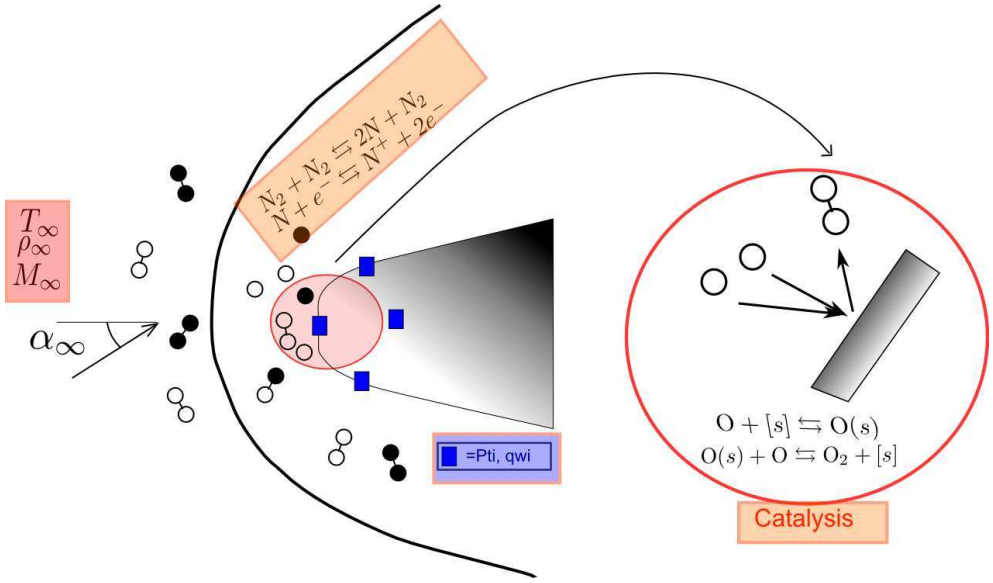

Figure 1: RAFLEX Flush Air Data System (FADS), sensors indicated in blue are flush mounted in the thermal protection system to measure the static pressure (pressure taps) and heat flux (calorimeters).

Flow conditions	Altitude [km]	T_∞ [K]	p_∞ [Pa]	M_∞ [-]
Chemical non-equilibrium	60	245.5	20.3	15.5

Table 1: Freestream conditions for one trajectory point of the EXPERT vehicle.

inverse problem based on a Bayesian setting, that is, probability densities of possible values of freestream conditions are rebuilt from stagnation-point pressure and heat flux measurements. A Bayesian setting offers a rigorous foundation for inferring input parameters from noisy data and uncertain forward models, a natural mechanism for incorporating prior information, and a quantitative assessment of uncertainty on the inferred results [7, 8]. It has already been used in the context of atmospheric entry for turbulence modeling calibration [9] and atomic nitrogen ionization modeling calibration [10].

In Section 2, the forward model and the associated numerical code are briefly described, as well as the different sources of uncertainty on input data. The latters are parametrized with random variables and propagated into the forward model using a non-intrusive polynomial chaos method [11, 12, 13]. The impact of the different uncertainties on the stagnation-point measurements is then studied through a sensitivity analysis based on the metamodel obtained with the stochastic spectral method. In Section 3, the new backward uncertainty propagation method is described, considering measurement errors and the input uncertainties that have the most impact.

2 Forward problem and sensitivity analysis

2.1 Physical problem

2.1.1 Governing equations

Here, the quantities of interest are the pressure $p_{\rm st}$ and heat flux $q_{\rm st}$ at the stagnation point. We use a set of physico-chemical models to simulate high temperature reacting flows, including 2D axi-symmetric Navier Stokes equations and gas/surface interaction equations (see Ref. [4]). Indeed, the wall of the spacecraft acts as a catalyzer and promotes recombination of atoms. This phenomenon is modeled by a catalytic wall at radiative equilibrium, where the so-called effective catalytic recombination coefficient γ represents the proportion of gas impinging the body that will recombine. A mixture of 5 species of air is used, namely N, O, N_2, O_2, and NO, with chemical mechanism due to Park [14]. Input data for the forward model are the freestream pressure p_∞ and Mach number M_∞, the effective catalytic recombination coefficient γ, and the gas reaction rate coefficients $k_{\rm r}$ of the chemical reactions r.

2.1.2 Sources of uncertainty

Uncertainties are considered on p_∞, M_∞, and γ, with uniform distributions detailed in Table 2. Concerning p_∞ and M_∞, only a priori ranges of plausible values are known. Concerning γ, the mean value corresponds roughly to the EXPERT material, while the 33% error have been previously determined [15].

Variable	Distribution	Min	Max
p_∞ [Pa]	Uniform	16.3	24.3
M_∞ [-]	Uniform	13.7	17.3
γ [-]	Uniform	0.001	0.002

Table 2: Distributions of M_∞, p_∞, and γ

Uncertainty is also considered on the gas reaction rate coefficients $k_{\rm r}$ of four chemical reactions of the dissociation reaction. To determine which reactions need to be accounted for, a preliminary triage was done using a 1D code to simulate the stagnation line shock layer chemistry [16]. For the trajectory point investigated, the dissociation reaction of molecular oxygen and nitric oxide was found important. Following the suggestion of Bose *et al.*[17], the uncertainty concerns only the pre-exponential factor $A_{\rm r}$ of the Arrhenius rate equation: $k_{\rm r} = A_{\rm r} T^{b_{\rm r}} \exp(-E_{\rm r}/RT)$. Since the uncertainties on $k_{\rm r}$ can be quite large, it is appropriate to consider them on a logarithmic scale ; in particular, $\log_{10}(k_{\rm r}/k_{\rm r,0})$, with $k_{\rm r,0}$ the recommended rate constant, is commonly assumed to vary following a normal distribution, with probability distribution defined by:

$$P(k_{\rm r}) \propto \exp\left[-\frac{1}{2}\left(\frac{\log_{10}(k_{\rm r}/k_{\rm r,0})}{\sigma_{\rm r}}\right)^2\right] \tag{1}$$

where $\pm 2\sigma_{\rm r}$ (reported in Table 3) defines the 95% confidence limits symmetrically bounding $k_{\rm r,0}$.

2.2 Numerical tools

2.2.1 COSMIC

To simulate the forward problem we use the in-house code COSMIC developed by Barbante [4]. This solver was designed to approximate hypersonic flow models where chemical non-equilibrium

Gas reaction	Distribution of $\log_{10} k_{\mathrm{r}}$	σ_{r}
$NO + O \rightarrow N + O + O$	Normal	0.12
$NO + N \rightarrow N + O + N$	Normal	0.12
$O_2 + N_2 \rightarrow 2O + N_2$	Normal	0.10
$O_2 + O \rightarrow 2O + O$	Normal	0.10

Table 3: Distributions of $\log_{10} k_{\mathrm{r}}$

effects need to be accounted for. It includes a Hybrid Upwind Splitting (HUS) scheme [18], which is an interesting attempt of combining, in a mathematically rigorous way, Flux Vector Splitting (FVS) and Flux Difference Splitting (FDS) schemes. The design principle combines the robustness of FVS schemes in the capture of nonlinear waves and the accuracy of some FDS schemes in the resolution of linear waves. In particular, COSMIC uses the hybridization of the Van Leer scheme [19] and the Osher scheme [20] and includes a carbuncle fix.

The boundary conditions are illustrated in the right panel of Figure 2 : an axi-symmetric condition is imposed on the y axis, while the wall of the body is modelled by a partially catalytic wall at radiative equilibrium. The mesh used for the computations is given in the right panel of Figure 2. Pressure and temperature iso-contours of the flow around EXPERT obtained with COSMIC for input data mean values are shown in Figure 3.

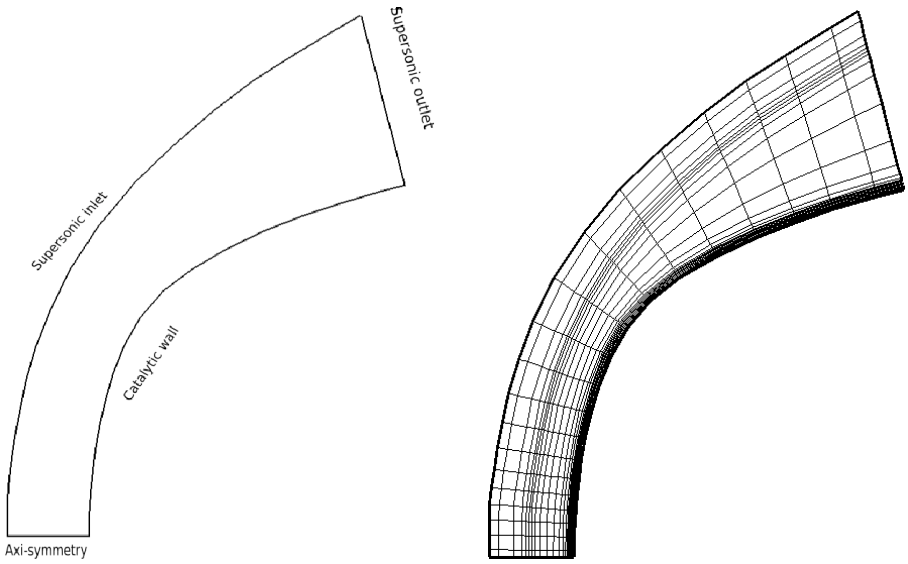

Figure 2: Boundary conditions (left) and mesh (right)

2.2.2 Uncertainty Quantification

The stochastic method used in this work to deal with the forward uncertainty quantification is the non-intrusive polynomial chaos, as implemented in the NISP (Non Intrusive Spectral Projection)

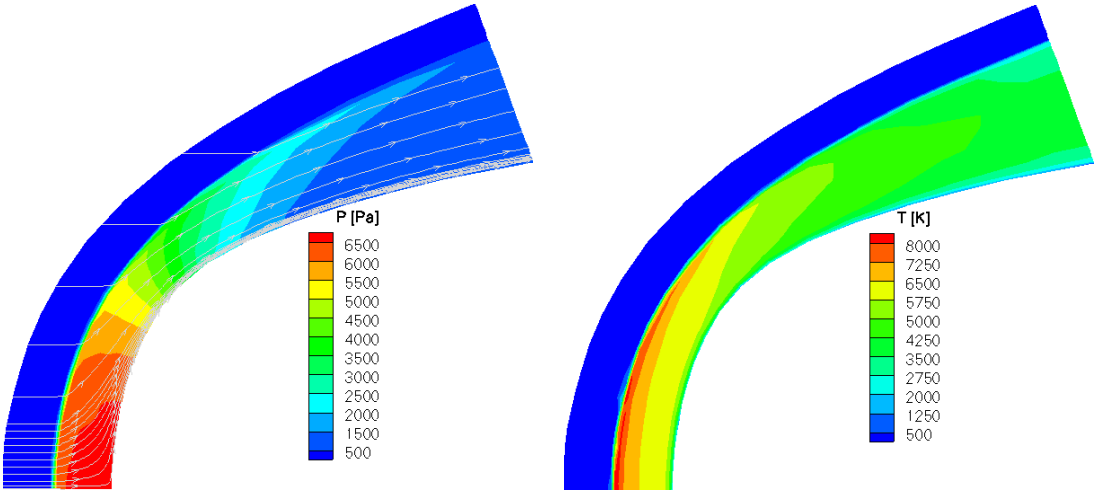

Figure 3: Pressure and temperature iso-contours for input data mean values

library. The development of NISP has been supported by the French National Research Agency (ANR) in the context of the OPUS (Open Platform for Uncertainty treatment in Simulation) project (see Ref. [13] for details).

Using this non-intrusive uncertainty quantification tool means that a single deterministic computation is replaced with a whole set of such computations, each one of those being run for specific values of the uncertain conditions. The choice of the set depends on the specific methodology selected, while the size of the set depends on the number of uncertain parameters that needs to be taken into account and the accuracy required on the solution of the stochastic problem. The coupling between the NISP UQ library and available flow solvers has been performed and described in Ref. [13].

Polynomial Chaos (PC) expansions are derived from the original theory of Wiener on spectral representation of stochastic processes using Gaussian random variables. Let $\boldsymbol{\xi}$ be a vector of standard independent random variables $\xi_i, i = 1, 2, ..., n_\xi$. Any well-behaved process u (with finite variance) can be expanded in a convergent (in the mean square sense) series of the form

$$u(\mathbf{x}, t, \boldsymbol{\xi}) = \sum_{\alpha} u_\alpha(\mathbf{x}, t)\Psi_\alpha(\boldsymbol{\xi}), \tag{2}$$

where α are multi-indices, $\alpha = (\alpha_1, \alpha_2, ..., \alpha_n)$, with each component $\alpha_i = 0, 1, ...,$ and Ψ_α are multivariate polynomial functions orthogonal with respect to the probability distribution function of the vector $\boldsymbol{\xi}$. Each Ψ_α is defined by a product of orthogonal polynomials $\Phi_i^{\alpha_i}(\xi_i)$, that is, $\Psi_\alpha(\boldsymbol{\xi}) = \prod_{i=1}^{n_\xi} \Phi_i^{\alpha_i}(\xi_i)$, where each $\Phi_i^{\alpha_i}$ is a polynomial of degree α_i, so that the degree of Ψ_α is $|\alpha|_1 = \sum_{i=1}^{n_\xi} \alpha_i$. A one-to-one correspondence exists between the choice of stochastic variable ξ_i and the polynomials $\Phi_i^{\alpha_i}(\xi_i)$. For instance, if ξ_i is a normal/uniform variable, the corresponding $\Phi_i^{\alpha_i}(\xi_i)$ are Hermite/Legendre polynomials of degree α_i. Coefficients $u_\alpha(x, t)$ are called the PC coefficients of the random process u and are obtained by

$$u_\alpha(\mathbf{x}, t) = \langle u(\mathbf{x}, t), \Psi_\alpha \rangle \, \|\Psi_\alpha\|^{-2}, \tag{3}$$

where the scalar product is defined by the expectation operator. For practical use, the PC

expansions are truncated to degree No

$$u(\mathbf{x}, t, \boldsymbol{\xi}) = \sum_{|\alpha|_1 \leq \mathrm{No}} u_\alpha(\mathbf{x}, t)\Psi_\alpha(\boldsymbol{\xi}). \tag{4}$$

The number of multivariate polynomials Ψ_α , that is, the dimension of the expansion basis, is related to the stochastic dimension n_ξ and the degree No of polynomials ; it is given by the formula $(n_\xi + \mathrm{No})!/(n_\xi!\mathrm{No}!)$.

Several approaches can be used to estimate PC coefficients. The approach used in this study is based on quadrature formulae, namely a non-intrusive formulation (see Ref.[11, 12] for details). When the number n_ξ of variables is large, quadrature formulae based on tensor product of a 1D formula require too many numerical evaluations and Sparse Grid integration based on Smolyak's construction is preferred. The PC coefficients are evaluated from a set of abscissas and weights $(\boldsymbol{\xi}_i, \omega_i)$ by formulae of the form

$$u_\alpha(\mathbf{x}, t) = \|\Psi_\alpha\|^{-2} \sum_{i=1}^{n} u(\mathbf{x}, t, \boldsymbol{\xi}_i)\Psi_\alpha(\xi_i)\omega_i. \tag{5}$$

From the PC expansion of the random process, it is then easy to derive its mean and variance and to estimate sensitivity information using the analysis of variance (ANOVA) decomposition [21].

2.3 Numerical results

Propagation of the uncertainties into the forward model has been performed with NISP using different polynomial orders No and a Smolyak Fejer quadrature formula of level 6, thus requiring 18943 resolutions of the deterministic code. Means and variances of p_{st} and q_{st} are reported in Table 4, while Sobol first order indices S_i and total order indices $S_{T,i}$ are reported in Table 5.

	p_{st}			q_{st}		
	$\mathrm{No} = 2$	$\mathrm{No} = 3$	$\mathrm{No} = 4$	$\mathrm{No} = 2$	$\mathrm{No} = 3$	$\mathrm{No} = 4$
μ	$6.49 \cdot 10^3$	$6.49 \cdot 10^3$	$6.49 \cdot 10^3$	$2.75 \cdot 10^5$	$2.75 \cdot 10^5$	$2.75 \cdot 10^5$
σ^2	$1.36 \cdot 10^6$	$1.37 \cdot 10^6$	$1.39 \cdot 10^6$	$9.73 \cdot 10^9$	$2.01 \cdot 10^{10}$	$6.18 \cdot 10^{10}$

Table 4: Means (μ) and variances (σ^2) of p_{st} and q_{st} for $\mathrm{No} = 2, 3, 4$

According to Table 4, the sensitivity analysis of the stagnation pressure p_{st} and of the stagnation heat flux q_{st} is convergent with respect to No. The interpretation of the indices S_i and $S_{T,i}$ is the following : X_i is an influential input parameter if S_i is important, whereas X_i is not an influential parameter if $S_{T,i}$ is small. Moreover, S_i close to $S_{T,i}$ means that interactions between X_i and the other parameters are negligible. From Table 5, p_∞ and M_∞ are observed to have the largest impact on p_{st} with an equivalent magnitude, whereas the effective recombination factor and the reaction rate coefficients have a very small effect on p_{st}, as expected. Moreover, interactions between p_∞ and M_∞ are negligible. The results are rather different when the heat flux is considered: all the inputs are observed to have a non negligible impact on q_{st}, with relatively equivalent orders of magnitude for p_∞, M_∞, γ, k_6, k_7, and smaller orders of magnitude for k_4 and k_5. Moreover, interactions between the different parameters are quite large. Finally, important coefficients of variation (ratio of the standard deviation to the mean) are observed on the stagnation pressure and heat flux: the value on p_{st} is 18%, whereas the value on q_{st} is approximately 52%. A possible way to reduce these uncertainties is to rebuild the probability densities of p_∞ and M_∞, which have an important impact on p_{st} and q_{st}.

		p_{st}			q_{st}		
		No $= 2$	No $= 3$	No $= 4$	No $= 2$	No $= 3$	No $= 4$
p_∞	S_1	$4.00 \cdot 10^{-1}$	$3.99 \cdot 10^{-1}$	$3.93 \cdot 10^{-1}$	$2.06 \cdot 10^{-2}$	$1.07 \cdot 10^{-2}$	$3.49 \cdot 10^{-3}$
	$S_{T,1}$	$4.09 \cdot 10^{-1}$	$4.07 \cdot 10^{-1}$	$4.02 \cdot 10^{-1}$	$3.38 \cdot 10^{-2}$	$6.18 \cdot 10^{-2}$	$4.91 \cdot 10^{-2}$
M_∞	S_2	$5.90 \cdot 10^{-1}$	$5.87 \cdot 10^{-1}$	$5.79 \cdot 10^{-1}$	$5.18 \cdot 10^{-1}$	$2.52 \cdot 10^{-1}$	$8.78 \cdot 10^{-2}$
	$S_{T,2}$	$5.98 \cdot 10^{-1}$	$5.99 \cdot 10^{-1}$	$5.91 \cdot 10^{-1}$	$5.28 \cdot 10^{-1}$	$7.14 \cdot 10^{-1}$	$2.81 \cdot 10^{-1}$
γ	S_3	$6.78 \cdot 10^{-4}$	$6.76 \cdot 10^{-4}$	$2.36 \cdot 10^{-3}$	$1.94 \cdot 10^{-1}$	$9.40 \cdot 10^{-2}$	$1.09 \cdot 10^{-1}$
	$S_{T,3}$	$6.79 \cdot 10^{-4}$	$2.30 \cdot 10^{-3}$	$1.22 \cdot 10^{-2}$	$1.94 \cdot 10^{-1}$	$3.03 \cdot 10^{-1}$	$5.44 \cdot 10^{-1}$
$O_2 + N_2 \rightarrow 2O + N_2$	S_4	$3.72 \cdot 10^{-6}$	$4.54 \cdot 10^{-6}$	$3.07 \cdot 10^{-5}$	$1.86 \cdot 10^{-3}$	$9.31 \cdot 10^{-4}$	$9.64 \cdot 10^{-4}$
	$S_{T,4}$	$2.76 \cdot 10^{-5}$	$1.65 \cdot 10^{-4}$	$8.33 \cdot 10^{-4}$	$7.52 \cdot 10^{-3}$	$2.70 \cdot 10^{-2}$	$3.98 \cdot 10^{-2}$
$O_2 + O \rightarrow 2O + O$	S_5	$2.65 \cdot 10^{-6}$	$3.90 \cdot 10^{-6}$	$1.98 \cdot 10^{-5}$	$1.10 \cdot 10^{-3}$	$6.35 \cdot 10^{-4}$	$5.47 \cdot 10^{-4}$
	$S_{T,5}$	$1.34 \cdot 10^{-5}$	$1.17 \cdot 10^{-4}$	$4.97 \cdot 10^{-4}$	$3.40 \cdot 10^{-3}$	$2.23 \cdot 10^{-2}$	$2.43 \cdot 10^{-2}$
$NO + O \rightarrow N + O + O$	S_6	$2.20 \cdot 10^{-4}$	$2.21 \cdot 10^{-4}$	$3.22 \cdot 10^{-4}$	$6.17 \cdot 10^{-2}$	$3.01 \cdot 10^{-2}$	$1.41 \cdot 10^{-2}$
	$S_{T,6}$	$2.53 \cdot 10^{-4}$	$7.56 \cdot 10^{-4}$	$5.88 \cdot 10^{-3}$	$7.02 \cdot 10^{-2}$	$1.02 \cdot 10^{-1}$	$2.50 \cdot 10^{-1}$
$NO + N \rightarrow N + O + N$	S_7	$6.60 \cdot 10^{-4}$	$6.58 \cdot 10^{-4}$	$2.33 \cdot 10^{-3}$	$1.83 \cdot 10^{-1}$	$8.86 \cdot 10^{-2}$	$1.04 \cdot 10^{-1}$
	$S_{T,7}$	$6.61 \cdot 10^{-4}$	$2.28 \cdot 10^{-3}$	$1.21 \cdot 10^{-2}$	$1.83 \cdot 10^{-1}$	$3.00 \cdot 10^{-1}$	$5.36 \cdot 10^{-1}$

Table 5: Sobol first order (S_i) and total order indices ($S_{T,i}$) for No $= 2, 3, 4$

3 Backward uncertainty propagation method

The purpose of this section is to rebuild the probability densities of the freestream conditions p_∞ and M_∞ from noisy observations of stagnation pressure p_{st} and heat flux q_{st}, by taking into account only the influence of measurement uncertainty concerning p_{st} and the influence of measurement and chemistry uncertainty concerning q_{st}.

3.1 Bayesian inference for inverse problems

The output of Bayesian inference is not a single value for the model parameters, but a posterior probability distribution that summarizes all available information about parameters. From this distribution, one can calculate means, modes, and high-order moments, compute marginal distributions, or make additional predictions by averaging over the posterior.

Let F denote the forward mathematics model defined as follows : $\mathbf{d} = F(\mathbf{m}, \mathbf{c})$, which yields predictions of the stagnation pressure and heat flux $\mathbf{d} = (p_{\text{st}}, q_{\text{st}})$ as a function of the freestream conditions $\mathbf{m} = (p_\infty, M_\infty)$ and the chemistry coefficients $\mathbf{c} = (\gamma, (k_{\text{r}})_{\text{r}=1,2,3,4})$. The uncertainty on $\mathbf{c}$ is assumed to be known and to follow a distribution $p_{\mathbf{c}}(\mathbf{c}) = p_\gamma(\gamma) \prod_{r=1}^{4} p_{k_{\text{r}}}(k_{\text{r}})$, γ following a uniform distribution detailed in Table 2 and k_{r} following lognormal distributions detailed in Table 3. In the Bayesian setting, both $\mathbf{m}$ and $\mathbf{d}$ are random variables and we use Bayes' rule to define a posterior probability density for the model parameters $\mathbf{m}$, given n observations of the data $\{\mathbf{d}^1, \ldots, \mathbf{d}^n\}$:

$$p(\mathbf{m}|\mathbf{d}^1, \ldots, \mathbf{d}^n) = \frac{p(\mathbf{d}^1, \ldots, \mathbf{d}^n|\mathbf{m}, \mathbf{c}) p_{\mathbf{m}}(\mathbf{m}) p_{\mathbf{c}}(\mathbf{c})}{\int p(\mathbf{d}^1, \ldots, \mathbf{d}^n|\mathbf{m}, \mathbf{c}) p_{\mathbf{m}}(\mathbf{m}) p_{\mathbf{c}}(\mathbf{c}) \mathrm{d}\mathbf{m}\mathrm{d}\mathbf{c}}. \tag{6}$$

Prior probability $p_{\mathbf{m}}(\mathbf{m})$ represents the degree of belief about possible values of $\mathbf{m} = (p_\infty, M_\infty)$ before observing any data ; p_∞ and M_∞ are a priori assumed to follow uniform distributions, with minima and maxima given in Table 2. Data then enters the formulation through the likelihood or joint density of the observations given $\mathbf{m}$ and $\mathbf{c}$, namely $p(\mathbf{d}^1, \ldots, \mathbf{d}^m|\mathbf{m}, \mathbf{c})$. A common model

assumes independent observations so that independent additive errors account for the deviation between predicted and observed values of $\mathbf{d}$:

$$\mathbf{d}^j = F(\mathbf{m}, \mathbf{c}) + \boldsymbol{\eta}^j, \quad j = 1, \dots, n. \tag{7}$$

Because p_{st} and q_{st} can be considered as independent, a typical assumption is that errors are realizations of a Gaussian random variable $\boldsymbol{\eta}^j \sim \mathcal{N}(\mathbf{0}, \boldsymbol{\Gamma})$, where $\boldsymbol{\Gamma} = \text{diag}(\sigma^2_{p_{\text{st}}}, \sigma^2_{q_{\text{st}}})$, $\sigma_{p_{\text{st}}}$ and $\sigma_{q_{\text{st}}}$ encompassing measurement errors. In that case, $\mathbf{d}^j|\mathbf{m}, \mathbf{c} \sim \mathcal{N}(F(\mathbf{m}, \mathbf{c}), \boldsymbol{\Gamma})$, and the likelihood is

$$p(\mathbf{d}^1, \dots, \mathbf{d}^m|\mathbf{m}, \mathbf{c}) = \prod_{j=1}^{n} p_{\mathbf{d}^j}(\mathbf{d}^j|\mathbf{m}, \mathbf{c}) = \prod_{j=1}^{n} p_{\boldsymbol{\eta}}(\mathbf{d}^j - F(\mathbf{m}, \mathbf{c}), \boldsymbol{\Gamma}), \tag{8}$$

with $p_{\boldsymbol{\eta}}$ the Gaussian density probability of $\mathcal{N}(\mathbf{0}, \boldsymbol{\Gamma})$. Since in general measurement errors are not known with exactness, one can consider $\boldsymbol{\sigma}_{\text{st}} = (\sigma_{p_{\text{st}}}, \sigma_{q_{\text{st}}})$ as hyperparameters of the Bayesian setting that needs to be inferred, with noninformative uniform a priori on $\sigma_{p_{\text{st}}}$ and $\sigma_{q_{\text{st}}}$. For simplicity, measurement errors are here assumed to be known, with $\sigma_{p_{\text{st}}} = 0.1\mu(p_{\text{st}})$ and $\sigma_{q_{\text{st}}} = 0.1\mu(q_{\text{st}})$.

3.2 Markov Chain Monte Carlo

Markov Chain Monte Carlo (MCMC) encompasses a broad class of methods that simulate drawing samples from the normalized posterior [22]:

$$p(\mathbf{m}|\mathbf{d}^1, \dots, \mathbf{d}^n) \propto p(\mathbf{d}^1, \dots, \mathbf{d}^n|\mathbf{m}, \mathbf{c}) p_{\mathbf{m}}(\mathbf{m}) p_{\mathbf{c}}(\mathbf{c}), \tag{9}$$

thus avoiding complex numerical integrations in high dimensions to form the posterior distribution. In this work, we use the Metropolis-Hastings algorithm with single-site updating and Gaussian proposal density to draw samples of $p(\mathbf{m}|\mathbf{d}^1, \dots, \mathbf{d}^n)$ and process as follow :

0. initialize the chain state $\mathbf{m}^{k=0} = (p_\infty^{k=0}, M_\infty^{k=0}) = (\mu(p_\infty), \mu(M_\infty))$
1.a generate $\mathbf{c}^{k,1}$ and a candidate $\widetilde{p}_\infty \sim \mathcal{N}(p_\infty^k, \omega^2_{p_\infty})$
1.b evaluate the acceptance rate $\alpha(p_\infty^k, \widetilde{p}_\infty) = \min\left\{1, \frac{p(\mathbf{d}^1,\dots,\mathbf{d}^n|\widetilde{p}_\infty, M_\infty^k, \mathbf{c}^{k,1}) p_{p_\infty}(\widetilde{p}_\infty)}{p(\mathbf{d}^1,\dots,\mathbf{d}^n|p_\infty^k, M_\infty^k, \mathbf{c}^{k,1}) p_{p_\infty}(p_\infty^k)}\right\}$
1.c generate $u^{k,1} \sim \mathcal{U}(0,1)$ and update: if $u^{k,1} < \alpha(p_\infty^k, \widetilde{p}_\infty)$, $p_\infty^{k+1} = \widetilde{p}_\infty$, else $p_\infty^{k+1} = p_\infty^k$
2.a generate $\mathbf{c}^{k,2}$ and a candidate $\widetilde{M}_\infty \sim \mathcal{N}(M_\infty^k, \omega^2_{M_\infty})$
2.b evaluate the acceptance rate $\alpha(M_\infty^k, \widetilde{M}_\infty) = \min\left\{1, \frac{p(\mathbf{d}^1,\dots,\mathbf{d}^n|p_\infty^{k+1}, \widetilde{M}_\infty, \mathbf{c}^{k,2}) p_{M_\infty}(\widetilde{M}_\infty)}{p(\mathbf{d}^1,\dots,\mathbf{d}^n|p_\infty^{k+1}, M_\infty^k, \mathbf{c}^{k,2}) p_{M_\infty}(M_\infty^k)}\right\}$
2.c generate $u^{k,2} \sim \mathcal{U}(0,1)$ and update: if $u^k < \alpha(M_\infty^k, \widetilde{M}_\infty)$, $M_\infty^{k+1} = \widetilde{M}_\infty$, else $M_\infty^{k+1} = M_\infty^k$
3. $k = k+1$, go to 1.a while $k < N_{\text{MCMC}}$, with N_{MCMC} a predefined number of times.

Regardless of the initial chain state, the above algorithm produces a Markov chain that converges to the posterior distribution ; the initial chain state values are here choosen to be the a priori mean values of each component. Nevertheless, the proposal distribution widths vector $\boldsymbol{\omega} = (\omega_{p_\infty}, \omega_{M_\infty})$ have to be chosen carefully in order for the chain to mix well and represent the full posterior distribution in the given number of MCMC steps. If the proposal distribution widths are too large, a great proportion of the proposed moves will be rejected, and the chain will not move very often. On the other hand, if they are too small, most proposed moves will be accepted but the chain will move very slowly through the posterior support. A way to choose $\boldsymbol{\omega}$ efficiently is to plot the empirical autocorrelation at lag s, denoted by $\beta(s)$, for each component of the vector to infer and different proposal distribution widths. Indeed, the

autocorrelation quantifies the interdependence of the iterations of a stochastic process, so that an efficient proposal distribution width implies the quickly decay of the autocorrelation with lag along the chain.

In steps 1.b and 2.b, $F(\widetilde{p}_\infty, M_\infty^k, \mathbf{c}^{k,1})$ and $F(p_\infty^{k+1}, \widetilde{M}_\infty, \mathbf{c}^{k,2})$ needs to be computed. The problem is that we can not afford to call COSMIC two times for each iteration of the Markov Chain, since COSMIC is time-consuming (about one hour per simulation) and one needs some thousands of iterations to produce a good sample of the posterior. To tackle this issue, one can rely on a metamodel, which gives an approximation of the outputs of COSMIC as a function of its inputs. Metamodels based on intrusive and non-intrusive stochastic spectral methods have already been proposed in the context of Bayesian inference[23, 24], with PC expansions as presented in 2.2.2. Thanks to the NISP toolbox, PC expansion metamodel functions of the form (4) can be obtained, providing an approximation of the response $(p_{\text{st}}, q_{\text{st}})$ as a function of $(\mathbf{m}, \mathbf{c})$. In Figure 4, approximated response surfaces of p_{st} and q_{st} are represented as a function of p_∞ and M_∞ in the top panels, the chemical inputs being fixed to their mean values ; then as a function of $\log_{10}(k_1/k_{1,0})$ and $\log_{10}(k_3/k_{3,0})$ in the bottom panels, the other inputs being fixed to their mean values. These response surfaces are obtained from the metamodels computed with the NISP toolbox, with the Sparse Grid integration method described in 2.3 and a PC expansion of order No = 3. The response surfaces of p_{st} are well approximated, this assertion was verified by plotting in the same graph the outputs provided by the resolutions of the COSMIC code in 2.3. The PC expansion of p_{st} can therefore be used as a metamodel. Moreover, these surfaces match with the results obtained in 2.3 : p_{st} variates significatively with p_∞ and M_∞, whereas it does not vary a lot with the chemical reaction rates (a similar behavior can be observed when plotting p_{st} as a function of γ, the other parameters fixed to their mean values). However, the response surfaces of q_{st} are not well approximated, because the values are not consistent with the ones obtained with COSMIC (the approximated response surface at the right top panel also reaches negative values, which is obviously unphysical). This behavior is explained by the fact that interactions between the different parameters are quite large (as pointed out in 2.3) and q_{st} strongly depends on all the parameters, so that a global polynomial approximation can not tackle every local variation, which results in an oscillatory behavior. The PC expansion of q_{st} can therefore not be used as a metamodel. Ongoing efforts consists in building a new metamodel for q_{st}, relying on adaptive local representations.

For this paper, it was decided to solve the stochastic inverse problem by considering only the stagnation-point pressure measurements $\{p_{\text{st}}^1, \ldots, p_{\text{st}}^n\}$, for which the PC expansion metamodel can be used. Since the chemical inputs have negligible impact on p_{st}, they are fixed to their mean values so that $\mathbf{c}$ does not appear any more in the MCMC algorithm. Moreover, the vector of observations $\{\mathbf{d}^1, \ldots, \mathbf{d}^n\}$ is reduced to $\{p_{\text{st}}^1, \ldots, p_{\text{st}}^n\}$ and we rely on a PC expansion metamodel of p_{st} in steps 1.b and 2.b to compute the likelihood. In order to improve the accuracy of the PC metamodel of p_{st}, a new metamodel is computed, which is only function of p_∞ and M_∞. This computation is performed with NISP using a polynomial order No = 3 and a full tensorized quadrature formula of level 6, requiring 36 resolutions of the deterministic code.

3.3 Numerical results

A noisy data vector $\{p_{\text{st}}^1, \ldots, p_{\text{st}}^{10}\}$ is generated by solving the forward model with COSMIC for a "true" vector of input parameters $(\mathbf{m}, \mathbf{c})$, then perturbing the output value p_{st} $n = 10$ times with independent samples of a Gaussian noise $\eta_i \sim \mathcal{N}(0, \sigma_{p_{\text{st}}}^2)$. For simplicity, $\sigma_{p_{\text{st}}}$ is supposed to be known (see 3.1). The "true" model parameters $\mathbf{m} = (p_\infty, M_\infty)$ is chosen as a sample of p_∞ and M_∞ from their prior (uniform) distributions, while the "true" chemistry coefficients $\mathbf{c} = (\gamma, (k_{\text{r}})_{r=1,2,3,4})$ is chosen as a sample of $p_{\mathbf{c}}$. The generated "true" values considered here

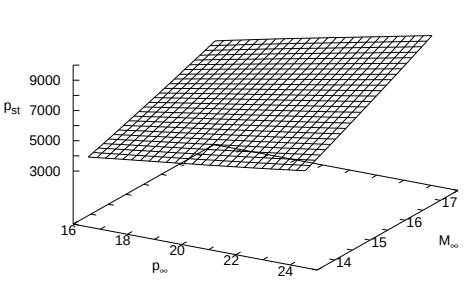

(a) p_{st} as a function of p_∞ and M_∞

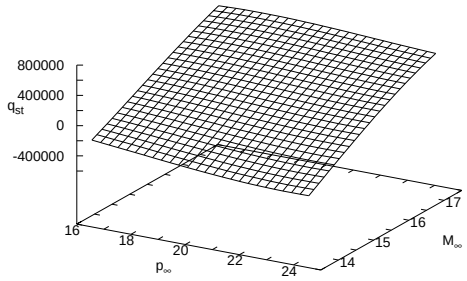

(b) q_{st} as a function of p_∞ and M_∞

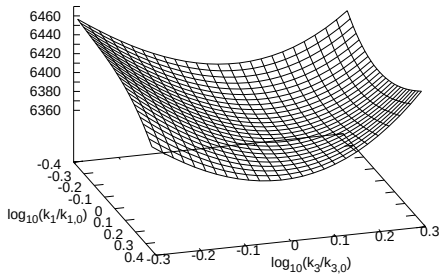

(c) p_{st} as a function of $\log_{10}(k_1/k_{1,0})$ and $\log_{10}(k_3/k_{3,0})$

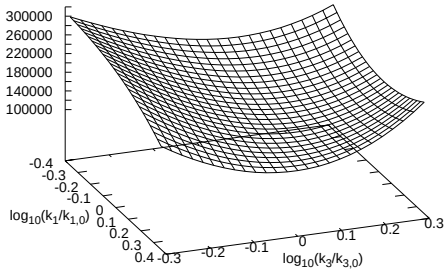

(d) q_{st} as a function of $\log_{10}(k_1/k_{1,0})$ and $\log_{10}(k_3/k_{3,0})$

Figure 4: Response surfaces of p_{st} and q_{st} obtained with the NISP toolbox, the Sparse Grid integration method described in 2.3, and a PC expansion of order No = 3

are $p_\infty = 19.65, M_\infty = 15, \gamma = 1.86 \cdot 10^{-3}, k_1 = 2.55 \cdot 10^{21}, k_2 = 1.03 \cdot 10^{22}, k_3 = 1.34 \cdot 10^{17}$, and $k_4 = 1 \cdot 10^{17}$. The output obtained for the latter inputs is $p_{\mathrm{st}} = 5.86 \cdot 10^3$ and perturbations of this "true" output, representing 10 independent measurements of p_{st} suffering from errors, can be observed in Figure 5. For information, if p_{st} is computed with the classical normal shock wave relations, neglecting the chemical effects and setting the adiabatic coefficient to 1.4, one obtains $p_{\mathrm{st}} = 5.702 \cdot 10^3$. This means a difference of 2.73%, which is non negligible.

A first graphical representation of the joint posterior density of (p_∞, M_∞) is obtained in Figure 6 by direct evaluations of the normalized posterior (9) on the prior intervals of p_∞ and M_∞, relying on the stagnation-point pressure metamodel. The joint density exhibits a ridge spread along a lightly curved line in the (p_∞, M_∞) plane. This density structure suggests a high degree of correlation between the two parameters, which is consistant with the physics of the system. Samples of the posterior $p(\mathbf{m}|p_{\mathrm{st}}^1, \ldots, p_{\mathrm{st}}^{10})$ are then computed through the above MCMC algorithm with a proposal distribution widths vector $\boldsymbol{\omega} = (\omega_{p_\infty}, \omega_{M_\infty}) = (0.9, 0.5)$. Results showing the chain position over 10000 iterations are reported in Figure 7, plotted in two dimensions and separately for p_∞ and M_∞. Visual inspection suggests that the chain mixes well and that it moves in the band of Figure 6 where the probability is nonzero. In Figure 8, the empirical autocorrelation at lag s, namely $\beta(s)$, is plotted for each component of $\mathbf{m}$

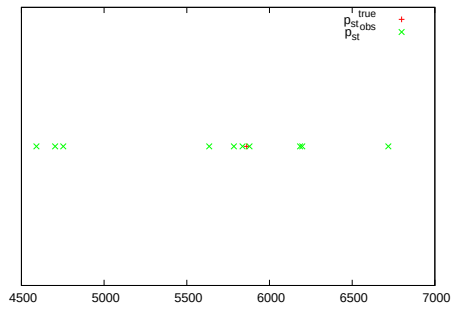

Figure 5: "True" p_{st} in red and 10 pseudo-measurements of $p_s t$ suffering from error in green

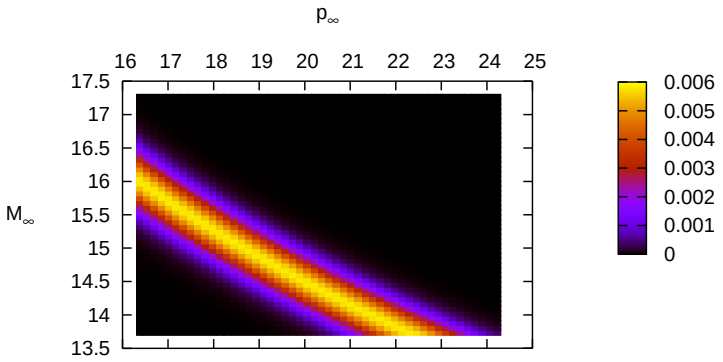

Figure 6: Joint posterior density of (p_∞, M_∞)

; $\beta(s)$ decays relatively quickly with lag along the chain, consistent with the good mixing in Figure 7. From Figures 6 and 7, it can be observed that the credible couples (p_∞, M_∞) set has been considerably reduced. However, a specific neighborhood around a MAP (Maximum A Posteriori) couple (p_∞, M_∞) has not been brought out, meaning that only measurements of p_{st} are not sufficient for determining the freestream conditions. In a future work, measurements of q_{st} along with an accurate metamodel for this quantity will be added so that such a more restricted region can be determined.

From the MCMC sample, the posterior distribution can be summarized in terms of means, standard deviations, and marginal distributions [22]. In order to approximate them, it is important to drop the first $(b-1)$ iterations of the MCMC sample, where b is commonly called the "burn-in" time, necessary for the chain to reach a good behavior. Let so consider $(p_\infty^k, M_\infty^k)_{k=b,\dots,K}$; the marginal mean and variance of p_∞ and M_∞ are estimated by

$$\overline{\mu}(p_\infty) = \frac{1}{K-b}\sum_{t=b+1}^{K} p_\infty^k, \quad \overline{\mu}(M_\infty) = \frac{1}{K-b}\sum_{t=b+1}^{K} M_\infty^k, \tag{10}$$

and

$$\overline{\sigma}^2(p_\infty) = \frac{1}{K-b-1}\sum_{t=b+1}^{K} (p_\infty^k - \overline{\mu}(p_\infty))^2, \quad \overline{\sigma}^2(M_\infty) = \frac{1}{K-b-1}\sum_{t=b+1}^{K} (M_\infty^k - \overline{\mu}(M_\infty))^2. \tag{11}$$

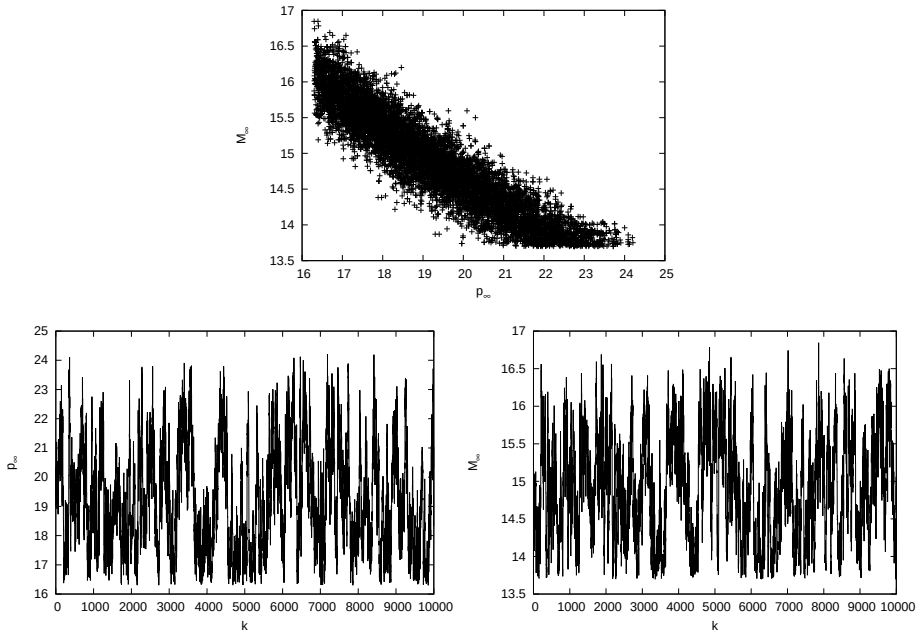

Figure 7: MCMC chain over 10000 iterations ; plotted in two dimensions and respectively for p_∞ and M_∞

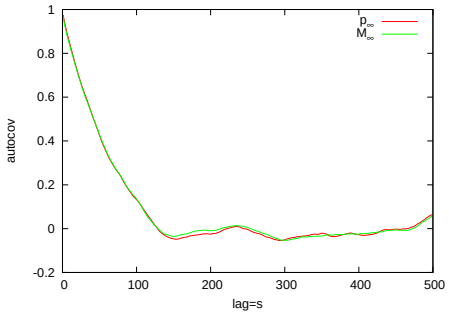

Figure 8: Empirical autocorrelation $\beta(s)$ for p_∞ in red and for M_∞ in green

The values obtained here are $\overline{\mu}(p_\infty) = 19.24$, $\overline{\mu}(M_\infty) = 14.93$, $\sigma(p_\infty) = 1.82$, and $\sigma(M_\infty) = 0.69$. The posterior means are roughly equal to the true ones, however the posterior standard deviations remains almost equivalent to the prior ones. This is consistent with the fact that some plausible couples (p_∞, M_∞) have been found in a lightly curved band in the (p_∞, M_∞) plane, so that each component have still a probability which is nonzero to belong to any point in the prior interval. A $100(1-2p)\%$ credible interval $[c_p, c_{1-p}]$ for p_∞ (resp. M_∞) can be estimated by setting c_p equal to the p^{th} quantile of $(p_\infty^k)_{k=b,\dots,K}$ (resp. $(M_\infty^k)_{k=b,\dots,K}$), and c_{1-p} equal to the $(1-p)^{th}$ quantile. The 95% credible intervals obtained here are $[16.49, 22.89]$ for p_∞ and $[13.76, 16.19]$ for M_∞. These intervals are observed to be slightly smaller than the prior ones. Finally, marginal

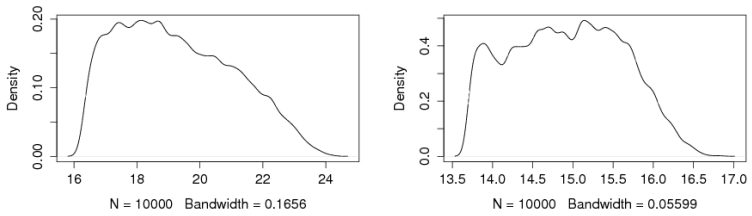

(a) Posterior distribution of p_∞ (b) Posterior distribution of M_∞

Figure 9: Marginal distributions of p_∞ and M_∞ obtained with kernel density estimation

distributions can be estimated by kernel density estimation :

$$p(p_\infty|p_{\rm st}^1,\dots,p_{\rm st}^{10}) \approx \frac{1}{K-b}\sum_{k=b+1}^{K}\mathcal{K}(p_\infty^k|\mathbf{m}^k), \quad p(M_\infty|p_{\rm st}^1,\dots,p_{\rm st}^{10}) \approx \frac{1}{K-b}\sum_{k=b+1}^{K}\mathcal{K}(M_\infty^k|\mathbf{m}^k), \tag{12}$$

where $K(p_\infty^k|\mathbf{m}^k)$ (resp. $K(M_\infty^k|\mathbf{m}^k)$) is a density concentrated around p_∞^k (resp. M_∞^k). Here we use a one-dimensional Gaussian kernel, $\mathcal{K}=\mathcal{N}(p_\infty^k,\omega^2)$ (resp. $\mathcal{K}=\mathcal{N}(M_\infty^k,\omega^2)$), with bandwith ω determined by the method of Sheather & Jones [25]. The estimated marginal distributions are plotted in Figure 9.

4 Conclusion

This paper deals with the reconstruction of the freestream conditions (p_∞, M_∞) for the trajectory of a re-entry vehicle from measurements of stagnation-point pressure and heat flux $(p_{\rm st}, q_{\rm st})$. Prior uniform distributions are first assumed for (p_∞, M_∞) and some chemistry parameters are considered uncertain, with known distribution functions. The impact of the different uncertain inputs on the forward problem simulated by the in-house code COSMIC is studied owing to a non-intrusive stochastic spectral method. Uncertainties on (p_∞, M_∞) are observed to have a large impact on $p_{\rm st}$, whereas the chemistry uncertainties are observed to have a negligible impact on it. On the contrary, all the input parameters are observed to have a considerable impact on $q_{\rm st}$. Then, a backward uncertainty propagation method is proposed to solve the inverse problem by taking into account uncertainties due to measurements and model parameters. To this end, we rely on a Bayesian framework supplied with MCMC algorithms to sample the posterior distribution of (p_∞, M_∞). A major difficulty lies in the fact that one needs to compute the forward problem for each iteration in the Markov chain. A metamodel for $p_{\rm st}$ is computed owing to the non-intrusive spectral method, unfortunately such a metamodel can not be obtained for $q_{\rm st}$ because of the large interactions between the different parameters and the strong dependence of $q_{\rm st}$ on all the parameters. It was therefore decided to solve the stochastic problem only relying on the stagnation pressure measurements and the metamodel for $p_{\rm st}$. The methodology exhibits a reduced set of credible couples (p_∞, M_∞) ; however a neighborhood around a Maximum A Posteriori credible couple has not been brought out, meaning that only stagnation point pressure measurements are not sufficient to determine freestream conditions. Ongoing efforts consists in building a new metamodel for $q_{\rm st}$, based on adaptive local representations, so as to add stagnation point heat flux measurements in the bayesian algorithm in an effective way.

Acknowledgments

This work was partially supported by the French National Research Agency (ANR) in the context of the UFO (Uncertainty quantification For compressible fluid dynamics and Optimisation) project.

Research of T. E. Magin is sponsored by the European Research Council Starting Grant #259354. This research was supported by the European Space Agency under contract ESA AO/1-6938/11/NL/SFE, technical monitor Dr. D. Giordano, and the European Office of Aerospace Research & Development, Air Force Office of Scientific Research, under grant FADS 11-3079, technical monitor Dr. G. Abate.

References

[1] M. J. Wright, D. Bose, and Y. K. Chen. Probabilistic modeling of aerothermal and thermal protection material response uncertainties. *AIAA Journal*, 45:399–410, 2007.

[2] G. Koppenwallner. Controlled Hypersonic Flight Air Data System and Flight Instrumentation. *Flight Experiments for Hypersonic Vehicle Development*, pages 17–1–17–30, 2008. Educational Notes RTO-EN-AVT-130, Paper 17.

[3] P. zur Nieden and H. Olivier. Determination of Atmospheric Densities from Reentry Data Flight Data. *Journal of Spacecraft and Rockets*, 44(2), 2007.

[4] P.F. Barbante. *Accurate and efficient modelling of high temperature non-equilibrium air flows*. PhD thesis, von Karman Institute, Rhode-Saint-Genèse, Belgium, 2001.

[5] M. J. Wright, D. Bose, G. E. Palmer, and E. Levin. Recommended collision integrals for transport property computations part 1: Air species. *AIAA Journal*, 43:2558–2564, 2005.

[6] J. Thoemel, J. Muylaert, F. Ratti, and J. Gavira. In-flight testing of critical technologies and experimentation of aerothermodynamic phenomena. In *Proceedings of the 16th AIAA/DLR/DGLR International Space Planes and Hypersonic Systems and Technologies Conference*, Bremen, Germany, 2009. American Institute of Aeronautics and Astronautics.

[7] J. Kaipio and E. Somersalo. *Statistical and Computational Inverse Problems*. Applied Mathematical Sciences, Vol. 160. Springer, 2010.

[8] I. Park and R. V. Grandhi. Quantifying multiple types of uncertainty in physics-based simulation using bayesian model averaging. *AIAA Journal*, 49:1038–1045, 2011.

[9] S.H. Cheung, T.A. Oliver, E.E. Prudencio, S. Prudhomme, and R.D. Moser. Bayesian uncertainty analysis with applications to turbulence modeling. *Reliability Engineering and System Safety*, 2011.

[10] K. Miki, M. Panesi, E.E. Prudencio, and S. Prudhomme. Estimation of the nitrogen ionization reaction rate using electric arc shock tube data and bayesian model analysis. *Physics of Plasmas*, 19(2), 2012.

[11] R. Ghanem and P. Spanos. *Stochastic finite elements: a spectral approach*. Dover, 2003.

[12] O. Le Maître and O. Knio. *Spectral Methods for Uncertainty Quantification*. Springer, 2010.

[13] P.M. Congedo, C. Corre, and J.-M. Martinez. Shape optimization of an airfoil in a bzt flow with multiple-source uncertainties. *Computer Methods in Applied Mechanics and Engineering*, 200(1):216–232, 2011.

[14] C. Park, R.L. Jaffe, and H. Partridge. Chemical-Kinetic Parameters of Hyperbolic Earth Entry. *Journal of Thermophysics and Heat Transfer*, 15(1):76–90, 2001.

[15] N. Villedieu, F. Panerai, O. Chazot, and T.E. Magin. Uncertainty quantification for gas-surface interaction in plasmatron. *Specialists Meeting on Catalytic Gas Surface Interactions (AVT-199), Rhode-Saint-Genèse, Belgium*, 2012.

[16] N. Villedieu, J. Cappaert, J.P. Garcia Galache, and T.E. Magin. Uncertainty Quantification for characterization of high enthalpy facilities. *4th European Conference for Aerospace Sciences, St Petersburg, Russia*, 2011.

[17] D. Bose, M. Wright, and T. Gokçen. Uncertainty and Sensitivity Analysis of Thermochemical Modeling for Titan Atmospheric Entry. *37th AIAA Thermophysics Conference, Portland, Oregon*, 2004.

[18] F. Coquel and M.S. Liou. Hybrid Upwind Splitting Scheme by a Field-by-Field Decomposition. *NASA Tech. Memorandum 106823*, 1995.

[19] B. Van Leer. Towards the ultimate conservative difference scheme. V. A second-order sequel to godunov's method. *Journal of Computational Physics*, 32(1):101–136, 1979.

[20] S. Osher and F. Solomon. Upwind Difference Schemes for Hyperbolic Systems of Conservation Laws. *Mathematics of Computation*, 38(158):339–374, 1982.

[21] T. Crestaux, O. Le Maître, and J.-M. Martinez. Polynomial chaos expansion for sensitivity analysis. *Reliability Engineering and System Safety*, 94(7):1161–1172, 2009.

[22] W.R. Gilks, Sylvia Richardson, and D.J. Spiegelhalter. *Markov Chain Monte Carlo in Practice*. Chapman & Hall, 1996.

[23] Najm H.N. Marzouk Y.M. and L.A. Rahn. Stochastic spectral methods for efficient Bayesian solution of inverse problems. *Journal of Computational Physics*, 224:560–586, 2007.

[24] Marzouk Y.M. and X. Dongbin. A Stochastic Collocation Approach to Bayesian Inference of Inverse Problems. *Communications in Computational Physics*, 6(4):826–847, 2009.

[25] S. J. Sheather and M. C. Jones. A reliable data-based bandwidth selection method for kernel density estimation. *Journal of the Royal Statistical Society series B*, 53:683–690, 1991.

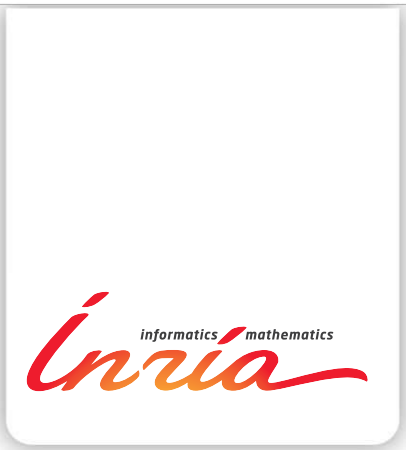

RESEARCH CENTRE
BORDEAUX – SUD-OUEST

351, Cours de la Libération
Bâtiment A 29
33405 Talence Cedex

Publisher
Inria
Domaine de Voluceau - Rocquencourt
BP 105 - 78153 Le Chesnay Cedex
inria.fr

ISSN 0249-6399